





Comparative analysis of the methods to compute the radiation term in Cummins' equation

José A. Armesto¹  · Raúl Guanche¹  · Fernando del Jesus¹ · Arantza Iturrioz¹  ·
Iñigo J. Losada¹ 

Received: 9 December 2014 / Accepted: 30 April 2015 / Published online: 13 June 2015
© Springer International Publishing AG 2015

Abstract In the present paper, the methods provided in literature to compute the convolution integral in Cummins' equation are compared. Direct computation of the convolution integral is revised to avoid truncation errors and to save computational cost. The three methods compared are the direct computation of the convolution integral, the approximation of the integral by a state space and the approximation of the impulse response function by Prony's coefficients. These methods are used to simulate the movement of the water inside an oscillating water column (OWC) and a decay test in heave of a spar buoy. Cummins' equation results in a system of ordinary differential equations with all the methods. All systems are computed using the same numerical scheme obtaining a fair comparison of the computational cost involved in each method. The results of the OWC are compared against CFD results and the results of the buoy against laboratory experiments. Results obtained by direct computation of the convolution integral show sensitivity to the time step used to precompute the impulse response function, while using state space or Prony's approximations are dependent on

the set of frequencies required for the identification of their coefficients. State space and Prony's approximations evaluate the radiation force, including it in the matrix of the system, while direct integration computes it outside of the matrix. This modification in the matrix makes these approximations more sensitive to the data used to evaluate the radiation force.

Keywords Cummins' equation · Radiation · Direct convolution integral · State space · Prony's approximation

1 Introduction

The movement of a floating structure in the time domain can be modelled by Cummins' equation (Cummins 1962). This equation takes into account information from the excitation forces produced by waves moving the structure and radiation forces produced by the movement of the structure itself, also known as fluid memory effect. Other external forces, such as those produced by moorings and power take off (PTO) systems, can also be included in the equation, but these forces are outside the scope of the present work. When the movement of the structure is only produced by incident waves, Cummins' equation is an order-two differential equation with a convolution integral in it. The presence of the convolution integral in Cummins' equation makes the solution complicated in the time domain (Kashiwagi 2004). There are methods in the literature to avoid this problem, which can be divided into two main families: approximation of the radiation term by a state space (Jefferys 1984), and approximation of the impulse response function (*irf*) by a sum of complex exponentials using Prony's method (Duclos et al. 2001; Paul 1998; de Prony 1795). A recent review of models used in the study of wave energy converters (WECs) is shown in Folley et al. (2012).

✉ Raúl Guanche
guancher@unican.es

José A. Armesto
armestoja@unican.es

Fernando del Jesus
dejesusf@unican.es

Arantza Iturrioz
iturrioz@unican.es

Iñigo J. Losada
losadai@unican.es

¹ Environmental Hydraulics Institute, "IH Cantabria",
Universidad de Cantabria, C/ Isabel Torres n 15 Parque
Científico y Tecnológico de Cantabria, 39011 Santander,
Spain

The first method to compute the convolution integral being considered in the present work is the direct solution of the convolution integral, hereinafter, IRF. Table 1 presents the abbreviations used throughout the paper. This method is reported as computationally expensive, as it has to be computed every time step with different data in the computation of the convolution integral. The common practice in literature to evaluate this infinite convolution integral is truncating it to a high enough value (Kurniawan et al. 2011; Perez and Fossen 2008; Ricci et al. 2008; Yu and Falnes 1995; Taghipour et al. 2008). Direct computation of the convolution integral is the method employed in commercial software SIMO (SIMO 2008), developed by Marintek, which has been used to evaluate the performance of different WECs (Babarit et al. 2012; Karimirad 2013; Muliawan et al. 2013). Another piece of software using the direct computation of the convolution integral is FAST (Jonkman 2007). This is a popular piece of software used to study wind turbines, including a module, HydroDyn, solving the hydrodynamics of floating wind turbines and directly integrating the convolution integral. It has been applied in Philippe et al. (2013), amongst others. The last FAST release, i.e. v8.03, includes also the solution of the radiation term approximated by state spaces as described in Duarte et al. (2013). In that work, the authors compare the results and computational costs, concluding that solving the convolution integral is not only more accurate, but also computationally more expensive than using state spaces. In order to save computational time, a change of variables can be used in the convolution integral, changing the scope of the functions. This change allows computation of the *irf* only once and storage of the results to be used in the computation of the convolution integral, instead of computing the *irf* every time the convolution integral is computed (Kurniawan et al. 2011).

The second method of approximation of the convolution integral considered in this work is approximation by a state space, a method hereinafter called SS. This method can be argued to be the most popular method to compute the convolution integral in Cummins' equation. Several approaches have been applied in the literature to identify the matrices of the state space and they can be classified into two main families: frequency domain methods (Jefferys 1984; McCabe et al. 2005) and time domain methods (Kristiansen and Ege-land 2003; Kristiansen et al. 2005; Yu and Falnes 1995, 1998). A review of these techniques can be found in Perez and Fossen (2008) and Taghipour et al. (2008). Recently, Perez and Fossen (2011) stated some important aspects that all methods identifying the coefficients applied to marine structures should fulfill. Applications of these methods can be found, for example, in the study of OWCs (Alves 2012; Iturrioz et al. 2014; Kurniawan et al. 2012), the study of one body heave converter involving control strategies (Abraham and Kerrigan 2013; Fusco and Ringwood 2011; Schoen et al.

Table 1 Abbreviations

Abbreviations	
ODE	Ordinary differential equation
OWC	Oscillating water column
WEC	Wave energy converter
<i>irf</i>	Impulse response function
IRF	Method used to compute the radiation term in Cummins' equation by direct integration of the convolution integral
SS	Method used to compute the radiation term in Cummins' equation by a state space
Prony	Method used to compute the radiation term in Cummins' equation by Prony's coefficients
RAO	Response amplitude operator
DOF	Degree of freedom
BEM	Boundary element method
TF	Transfer function
SWL	Still water level

2011) or the study of more than one body (de Andres et al. 2013; Yu et al. 2010). This method is also used in naval applications, for example in Spyrou and Tigkas (2011). As mentioned before, state spaces have been recently implemented to avoid solving the convolution integral in FAST (Duarte et al. 2013). Another model to study offshore floating vertical axis wind turbines (VAWTs), known as FloVAWT, which uses state space approximation, is presented by Shires et al. (2013).

The third method available in the literature to evaluate the convolution integral of Cummins' equation is the approximation of the *irf* by a sum of complex exponentials using Prony's method. Prony's method was developed by de Prony (1795), and it was applied to the approximation of the convolution integral by Duclos et al. (2001) and Paul (1998). This method is hereinafter called Prony. This methodology is used in the study of the SEAREV (Babarit and Clément 2006; Babarit et al. 2006) and to study a spar buoy used to extract wave energy (Grilli et al. 2007). More recently, it has also been used with a heaving buoy WEC (Bailey and Bryden 2012), a heaving buoy attached via a tether to a direct-drive generator (Crozier et al. 2013) and a submerged wave energy point absorber (Guanche et al. 2013).

This paper presents a comparative analysis of these available methods. Previous works (Kurniawan et al. 2011; Ricci et al. 2008; Taghipour et al. 2008) have presented similar studies where IRF and SS methods are compared. In Taghipour et al. (2008). Simulink is used to compute the problem embedding the solution of the convolution integral as an S-function with the trapezoidal integration method programmed in C. As a conclusion, SS approximation is reported

to be between 8 and 80 times faster than IRF. In Kurniawan et al. (2011), Matlab is used to calculate the convolution integral and different methods to evaluate the ODEs system generated by the SS method are tested. Kurniawan et al. (2011) conclude that IRF is slow, but the accuracy of the method is guaranteed when time step is small enough. In order to compute the *irf*, Kurniawan et al. (2011) truncate the infinite integral to a high-frequency value. This approach may yield errors if the truncating high frequency is not properly selected. In this article, this kind of error is avoided since the integral is analytically calculated until infinity (Kashiwagi 2000, 2004). In Ricci et al. (2008), the identification of state space is done in the time domain, while in this article this identification is done in the frequency domain following Perez and Fossen (2011). Furthermore, the resulting ODE system obtained using SS and Prony's method is computed using a 5th order Runge–Kutta method, while the direct integration of the radiation term is done using backward Euler and Crank–Nicholson methods. So far, the models used to compute the convolution integral have been always compared using different methods to obtain the solution of the resulting system of equations.

The purpose of this article was to summarise and compare the three methods used in the literature. The methods under study are the direct solution of the convolution integral, IRF, approximation of the convolution integral by state spaces, SS, and approximation of the *irf* by Prony's method, Prony. In this paper, the results obtained are compared using the same technique to calculate the resulting system of first-order ODEs.

The programs used to calculate the convolution integral by the three methods were written by the authors. In all three cases, the convolution integral, matrices and the computation of *irf* for a predefined set of times is done in Python and the results are written in files. Programs, made in Fortran, read these files and compute the ODEs using ODEPACK (Hindmarsh 1983), or VODE (Brown et al. 1989). Also, wave excitation force is computed in Python and saved into a file. This way, in the study of the movements of one WEC under several wave conditions, the only file that needs to be changed is the one containing the wave excitation force information. The matrices and *irf* information, if needed, would be computed only once for the complete set of wave conditions under study.

The computational cost, shown in tables throughout the paper, only contains the cost of the computation of the ODEs systems. Exceptionally, in the case of the response amplitude operator (RAO), the cost of the whole process is shown. The solution of the system provided by Prony's method contains complex values, so the complex version of VODE (Brown et al. 1989), ZVODE, is used. VODE is based on ODEPACK. A comparison between ODEPACK and VODE has been performed providing both the same results at very similar

computational costs. All computations have been performed in just one core and always in the same computer, a desktop computer. As ODEPACK and VODE use variable time step methods, the same restrictions to the computation of the time step were applied in all cases. Therefore, for the first time, the different techniques used to evaluate the convolution integral can be compared in a fair way in this work.

In this article, different methodologies have been applied to the study the OWC and a spar buoy. A first set of tests compare the results obtained in the study of an OWC, as presented by Iturrioz et al. (2014), with results from numerical models. Results and the computational effort required for each method are compared with data from an in-house CFD software IH-2VOF (Losada et al. 2008) and WADAM (WADAM 2014). The first study case in this paper is the comparison of the results with those of a decay test obtained with IH-2VOF. Decay tests are suitable for the purpose of comparing the methods in literature (IRF, SS and Prony) to evaluate the radiation term, as only radiation and hydrostatic forces are considered. The second test, used for the OWC, is to compare the RAO obtained from each method with the one calculated with WADAM. Finally, results are compared with those produced by IH-2VOF for irregular waves.

IH-2VOF evaluates the 2D Reynolds Averaged Navier–Stokes (RANS) equations (Liu et al. 1999; Hsu et al. 2002), based on the decomposition of the instantaneous velocity and pressure fields and the $k - \varepsilon$ equations for the turbulent kinetic energy (k) and the turbulent dissipation rate (ε). The model has been under a continuous development process based on an extensive validation procedure carried out for low-crested structures (Garcia et al. 2004; Losada et al. 2005; Lara et al. 2006), wave breaking on permeable slopes (Lara et al. 2006), overtopping on rubble mound breakwaters and low-mound breakwaters (Lara et al. 2008; Losada et al. 2008; Guanche et al. 2009), pore pressure damping in rubble mound breakwaters (Guanche et al. 2015) and the study of OWCs (Armesto et al. 2014; Iturrioz et al. 2014). The detailed validations provided by the aforementioned studies have tested the capability of the IH-2VOF model to satisfactorily reproduce the wave–structure interactions.

After the validations using the OWC, a second set of comparisons uses a decay test of the spar buoy based on the Hywind offshore wind project, and results from all methods are compared with results from laboratory. A sensitivity analysis is performed for the time step, the memory of the fluid and the frequencies obtained from different runs of WADAM.

This paper is organised in three parts. The first part describes the different numerical approximations considered: IRF, SS and Prony. In the second part, the results yielded by each of the methods are given and discussed. The last part presents the conclusions of the study.

2 Numerical model

Cummins’ equation is a differential equation of order two with a convolution integral that provides the movement of a floating structure in time domain. In the present paper, only the movements in one degree of freedom (DOF), heave, are considered. Therefore, Cummins’ equation can be written as

$$(M + A_\infty)\ddot{z}(t) + \int_0^t K(t - \tau)\dot{z}(\tau)d\tau + Cz(t) = F^{\text{exc}}(t), \tag{1}$$

where $z(t)$ is the heave position of the structure, M is the mass of the structure, A_∞ the added mass at infinity frequency, K the *irf*, also known as retardation function and fluid memory, C the restoring hydrostatic coefficient and F^{exc} the external forces, which can include wave forces, mooring forces, PTO forces, current forces, wind forces, etc. In this study, the only external forces used are the wave forces. The wave excitation forces are provided by the boundary element method (BEM) for the computed frequencies. In order to be able to reproduce realistic situations as those produced by IH-2VOF or at the laboratory, friction forces should be included in the model. The friction force is a hydrodynamic force that takes into account the viscous and turbulent losses produced at the submerged part of the body. Friction forces are included at the right-hand side of the Eq. (1). This friction force depends on the velocity of the movement and, in the adopted formulation (Iturrioz et al. 2014) it has two components, one linear and one nonlinear:

$$F_f(t) = k\dot{z}(t) = (k_1 + k_{nl}\dot{z}(t))|\dot{z}(t)|, \tag{2}$$

where k_1 is the linear coefficient and k_{nl} the nonlinear coefficient, which require calibration.

The three alternatives used in literature to compute the convolution integral in Cummins’ equation are reviewed in the following sections.

2.1 Solving the convolution integral (IRF method)

Before solving the convolution integral of Cummins’ equation, the *irf*, $K(t)$, needs to be computed. For every instant, t , the following infinite integral needs to be computed:

$$K(t) = \frac{2}{\pi} \int_0^\infty B(\omega) \cos(\omega t) d\omega, \tag{3}$$

where B is the damping coefficient for every frequency. In order to compute the previous value, damping coefficients are needed for all possible frequencies $\{B(\omega) : \omega \in [0, \infty)\}$. BEM, such as WAMIT/WADAM (WADAM 2014; WAMIT 2014) provides these coefficients for a set of predefined frequencies $\{\omega_n\}_{n=0}^N$. BEM models require more elements/panels as frequency grows. There is an upper limit

for the frequencies that produce accurate results for a given panel size of 8 panels per wavelength. The set of damping values, $\{B(\omega_n)\}_{n=0}^N$, can be extended to infinity by an exponential function (Kashiwagi 2000, 2004). A similar approach is proposed to extend the function by means of a geometric function in Greenhow (1986) and Perez and Fossen (2008). The effects of both extensions, exponential and geometric, are to increase the initial value of $K(t)$ and to smooth the function afterwards. This can be seen in Figure 2 for the exponential tail proposed by Kashiwagi (2000, 2004) and used in this work and in Figure 4 of Perez and Fossen (2008) for the geometric tail. This is achieved by finding the exponential function of form $ae^{b\omega}$ that better approximates the obtained values of the damping at given frequencies, $\{\omega_n\}_{n=0}^N$, in the sense of least square. The extended damping function, \hat{B} , can be expressed as

$$\hat{B}(\omega) = \begin{cases} B(\omega_i) & \text{for } \omega \leq \omega^* \\ ae^{b\omega} & \text{for } \omega > \omega^*. \end{cases} \tag{4}$$

The ω^* frequency is defined in this work as the crossing frequency between BEM data, $\{B(\omega_n)\}_{n=0}^N$, and the exponential, assuming that for high frequencies the data provided by BEM programs could be contaminated by the size of the panel (Kurniawan et al. 2011). Figure 1 shows the damping of the DOF heave for the volume of water trapped in the OWC studied by Iturrioz et al. (2014) and its extrapolating function (dashed line).

Truncating the infinite integral, to a high value of frequency, is common practice in the literature (Kurniawan et al. 2011; Perez and Fossen 2008; Ricci et al. 2008; Yu and Faldes 1995) to compute the *irf*. The solution adopted in this work

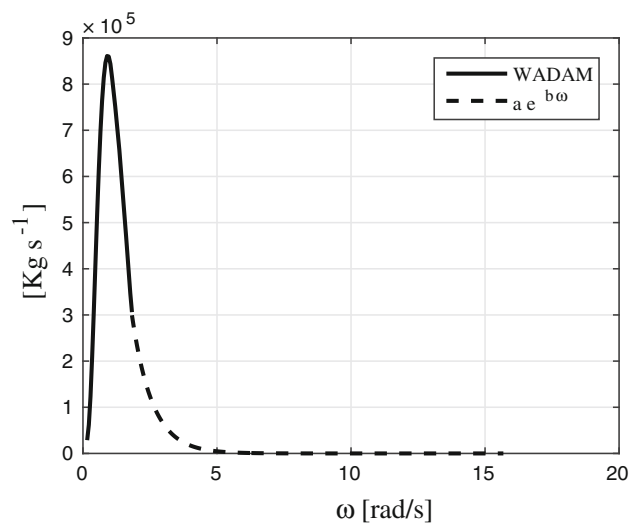


Fig. 1 Damping of the oscillating body in heave. *Continuous line* represents BEM data until the crossing frequency ω^* and *dashed line* represents the exponential function $ae^{b\omega}$ evaluated from ω^*

(Kashiwagi 2004) avoids the truncation, as the integral of the exponential function is analytically evaluated to infinity.

The first step to compute the *irf* is to split Eq. (3) into a finite integral and an infinite integral:

$$K(t) = \frac{2}{\pi} \int_0^\infty \hat{B}(\omega) \cos(\omega t) d\omega$$

$$= \frac{2}{\pi} \left[\int_0^{\omega^*} B(\omega) \cos(\omega t) d\omega + \int_{\omega^*}^\infty a e^{b\omega} \cos(\omega t) d\omega \right]. \tag{5}$$

The resulting finite integral can be calculated numerically, by means of the trapezoidal method, for example using `trapz` in Matlab or Python (`numpy`). The infinite integral has a finite result as the exponential is negative. A primitive, F , can be found applying twice integration by parts; see Appendix:

$$F(\omega) = \frac{\frac{a}{b} e^{b\omega} [\cos(\omega t) + \frac{t}{b} \sin(\omega t)]}{\left(1 + \frac{t^2}{b^2}\right)}. \tag{6}$$

This primitive goes to zero when ω goes to infinity; then,

$$\int_{\omega^*}^\infty a e^{b\omega} \cos(\omega t) d\omega = F(\omega)|_{\omega^*}^\infty = -F(\omega^*). \tag{7}$$

Consequently, it is possible to accurately compute the *irf* for every desired time without truncating the infinite integral in Eq. (3). For example, the OWC used in Iturrioz et al. (2014) is used in this study to illustrate the results. Figure 2 shows the *irf* for the heave of the considered body and for time $t \in [0, 10]$. The figure shows the value of each integral (finite and infinite) for every time step and the sum of both into the *irf*, $K(t)$. The error derived when truncating the infinite integral to the value of ω^* can be seen. It is clear that the *irf* is

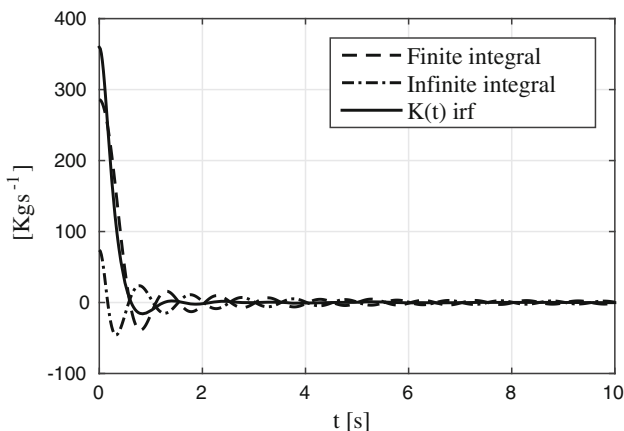


Fig. 2 Impulse response function $K(t)$ for the volume studied in Iturrioz et al. (2014) for $t \in [0, 10]$

significantly high at the beginning and negligible after 3s in this particular case. Then for $t > 3$, the *irf* can be neglected.

Therefore, the influence of the convolution integral, $I(t)$, is limited after a certain time t^* (Chitrapu and Ertekin 1995; de Kat 1988; Nolte and Ertekin 2014), which means that $K(t)$ can be neglected for $t > t^*$. Hence, $K(t - \tau)$ can be neglected for $\tau < t - t^*$, reducing the computational effort. Consequently,

$$I(t) = \int_0^t K(t - \tau) \dot{z}(\tau) d\tau = \int_0^{t-t^*} \overbrace{K(t - \tau) \dot{z}(\tau)}^{\approx 0} d\tau$$

$$+ \int_{t-t^*}^t K(t - \tau) \dot{z}(\tau) d\tau \approx \int_{t-t^*}^t K(t - \tau) \dot{z}(\tau) d\tau. \tag{8}$$

Applying a simple change of variables ($s = t - \tau$) to the last integral, Eq. (8) can be rewritten for a more convenient interval, $[0, t^*]$:

$$I(t) = \int_{t-t^*}^t K(t - \tau) \dot{z}(\tau) d\tau = \int_{t^*}^0 K(s) \dot{z}(t - s) (-ds)$$

$$= \int_0^{t^*} K(s) \dot{z}(t - s) ds. \tag{9}$$

To avoid computing the convolution integral every time step, a collection of values of $K(t)$ for $t \in [0, t^*]$ (using an appropriate Δt , can be precomputed), as done by Kurniawan et al. (2011). If $N = t^*/\Delta t$, the convolution integral can be rewritten applying the trapezoidal integration method, as done in Kashiwagi (2004) and Taghipour et al. (2008), as:

$$I(t) = \int_0^{t^*} K(s) \dot{z}(t - s) ds$$

$$= \Delta t \left[\frac{K(0) \dot{z}(t) + K(t^*) \dot{z}(t - t^*)}{2} \right.$$

$$\left. + \sum_{n=1}^{N-1} K(n\Delta t) \dot{z}(t - n\Delta t) \right]. \tag{10}$$

This way, the *irf* only needs to be computed once for a given set of time steps and can be applied to simulate every wave condition (Kurniawan et al. 2011). This implies a huge saving in computational effort, as the *irf* is not required to be computed every time step. This methodology can cause errors if Δt is not small enough, especially with rapid changes in \dot{z} , as is the case on studying waves close to the structure natural period.

Once the convolution integral, $I(t)$, is computed, Cummins' equation can be converted into a system of two first-order ODEs. Defining $k_1 = z$ and $k_2 = \dot{z}$, then Cummins' equation can be written as

$$\begin{aligned} \dot{k}_1(t) &= k_2(t) \\ \dot{k}_2(t) &= -\frac{I(t)}{M+A_\infty} - \frac{C}{M+A_\infty}k_1(t) + \frac{F^{\text{exc}}(t)}{M+A_\infty}. \end{aligned} \tag{11}$$

Finally, solving the Cummins’ equation, in (11) is equivalent to solving a system of first-order ODEs, which in this study is done by ODEPACK (Hindmarsh 1983) and VODE (Brown et al. 1989). The order of the system is twice the number of DOFs under study. In this case, one DOF is studied, so the order of the system is two.

2.2 Approximation of the convolution integral by a state space (SS method)

In the SS method, the convolution integral in Cummins’ equation, is approximated by a state space (Taghipour et al. 2008; Yu and Falnes 1995). The *irf* represents the memory of the fluid and using Laplace transformation it can be written as the transfer function (TF), $K(s)$, in the frequency domain. This TF is approximated in the frequency domain (Perez and Fossen 2009, 2011; Taghipour et al. 2008) by a parametric function, $\hat{K}(\omega)$, expressed as

$$K(s) \approx \hat{K}(s) = \frac{P(s, \omega)}{Q(s, \omega)} = \frac{p_m s^m + p_{m-1} s^{m-1} + \dots + p_0}{s^n + q_{n-1} s^{n-1} + \dots + q_0}, \tag{12}$$

where $s = i\omega$ is the Laplace complex variable. The coefficients of the polynomials $P(s, \omega)$ and $Q(s, \omega)$ are determined by means of a least square fitting to a set of known values. Those values are obtained from the application of the hydrodynamic BEM for a range of frequencies. The output obtained from BEM are the damping coefficients, $B(\omega)$, added mass coefficients, $A(\omega)$, and the added mass at infinite frequency, A_∞ . Then a set of $K_{\text{wadam}}(\omega)$ values can be defined:

$$K_{\text{wadam}}(i\omega) = B(\omega) + i[A(\omega) + A_\infty]. \tag{13}$$

TF in the frequency domain, $K(\omega)$, and *irf* in the time domain, $K(t)$, are related by a Fourier transform:

$$\hat{K}(i\omega) \approx K(i\omega) = \frac{2}{\pi} \int_0^\infty K(t) e^{-i\omega t} dt. \tag{14}$$

Figure 3 shows the approximation obtained in the case studied in Iturrioz et al. (2014).

For instance, the SS method is used to approximate the convolution integral $I(t)$ in Alves (2012), Iturrioz et al. (2014) and Yu and Falnes(1995, 1998). In Taghipour et al. (2008), different ways to express the linear equation systems are presented. It also includes the approximation of a convolution integral by a state space representation:

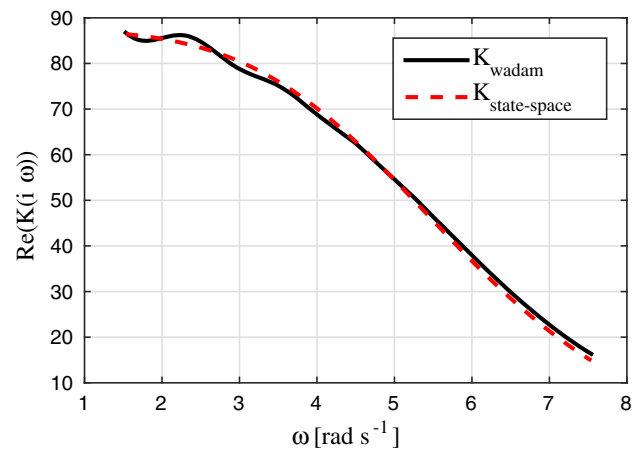


Fig. 3 Identification of TF, $K(i\omega)$, for the volume studied in Iturrioz et al. (2014)

$$\begin{aligned} \dot{x}_c(t) &= A_c x_c(t) + B_c u_c(t) \\ y_c(t) &= C_c x_c(t), \end{aligned} \tag{15}$$

where A_c is the state matrix, B_c the input matrix, C_c the output matrix, $x_c(t)$ the state vector, $u_c(t)$ the input vector and $y_c(t)$ the output vector of the state-space that approximates the convolution integral. The input of the system is the heave velocity of the body. These statements can be expressed as follows:

$$\begin{aligned} u_c(t) &= \dot{z}(t) \\ y_c(t) &\approx I(t) = \int_0^t K(t - \tau) \dot{z}(\tau) d\tau. \end{aligned} \tag{16}$$

The state and input and output matrices, given in Eq. (15), are built by conveniently placing the coefficients of the polynomials $P(s, \omega)$ and $Q(s, \omega)$ obtained in the TF approximation in them (Taghipour et al. 2008).

However, the heave velocity of the body, $\dot{z}(t)$, that feeds the convolution state space subsystem needs to be obtained from solving Cummins’ equation for every time step. For this purpose, another state space system will be defined: the general state space system (Alves 2012; Yu and Falnes 1995). It describes the general equation of motion of the body, taking into account all the forces considered in it (Cummins 1962), including the convolution integral, $I(t)$, by means of the convolution state space subsystem:

$$\begin{aligned} \dot{x}(t) &= Ax(t) + Bu(t) \\ y(t) &= Cx(t). \end{aligned} \tag{17}$$

In this general system, the input is the excitation force, $u(t) = F^{\text{exc}}(t)$, and the output is the heave displacement of the body, $y(t) = z(t)$. The input matrices A_c , B_c and C_c in Eq. (15) are included in general matrix A (Yu and Falnes 1995).

Once again, Cummins’ equation is written as a system of first-order ODEs. In this case, the order of the system is twice the number of DOFs under study plus the sum of the orders of all the state space equations used to approximate the convolution integral of every coupling of DOFs. For example, in the study of a 6 DOFs system, there are 36 convolution integrals to approximate, which may be reduced depending on the symmetry of the body.

2.3 Approximation of the convolution integral by Prony’s estimation (Prony method)

The *irf*, Eq. (3), can be approximated by a sum of exponential functions using Prony’s approximation (Duclos et al. 2001; Paul 1998). This method provides a set $\{\alpha_i, \beta_i\}_{i=1}^P \in \mathbb{C}^2$ such that

$$K(t) \approx \sum_{i=1}^P \alpha_i e^{\beta_i t}. \tag{18}$$

Figure 4 shows the approximation by Prony’s method of the *irf* presented in Fig. 2. Then the convolution integral can be approximated by

$$I(t) \approx \sum_{i=1}^P I_i(t), \tag{19}$$

where

$$I_i(t) = \int_0^t \alpha_i e^{\beta_i(t-\tau)} \dot{z}(\tau) d\tau; \quad i = 1, 2, \dots, P. \tag{20}$$

Using Leibniz’s integral rule it can be seen that

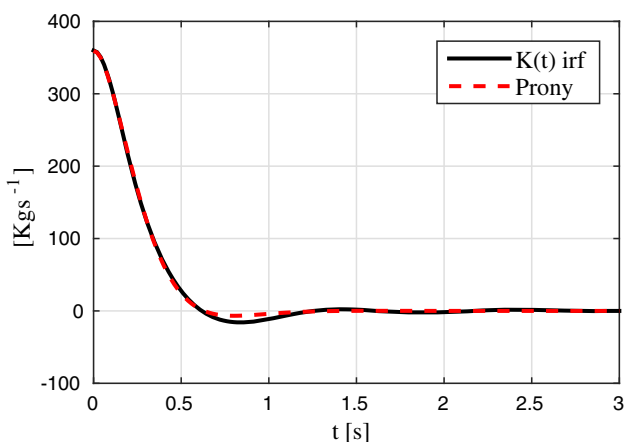


Fig. 4 Approximation by Prony’s method to the *irf*, $K(t)$, for the volume studied in Iturrioz et al. (2014) and $t \in [0, 3]$

$$\dot{I}_i(t) = \beta_i I_i(t) + \alpha_i \dot{z}(t), \quad i = 1, 2, \dots, P. \tag{21}$$

Equation (21) represents a system of first-order ODEs. Using the approximation from Eq. (19), Cummins’ equation can be written as

$$(M + A_\infty)\ddot{z}(t) + \sum_{i=1}^P I_i(t) + Cz(t) = F^{\text{exc}}(t). \tag{22}$$

Defining $k_1 = z$ and $k_2 = \dot{z}$, Cummins’ equation can be written as a system of two ODEs:

$$\begin{aligned} \dot{k}_1(t) &= k_2(t) \\ \dot{k}_2(t) &= -\frac{\sum_{i=1}^P I_i(t)}{M+A_\infty} - \frac{C}{M+A_\infty}k_1(t) + \frac{F^{\text{exc}}(t)}{M+A_\infty}. \end{aligned} \tag{23}$$

So, by writing together Eqs. (21) and (23), it can be concluded that solving Cummins’ equation is, once again, equivalent to solving a system of ODEs. In this case, the order of the system is twice the number of DOFs under study plus the sum of the orders of all the Prony’s functions used to approximate the convolution integral of every coupling of DOFs. Prony’s coefficients are complex values; therefore, a solver to deal with complex-valued ODE systems, such as ZVODE, is required. The imaginary part of the solution of the systems is smaller than 10^{-10} in all tested cases and it has been neglected.

3 Comparison

In order to compare the results yielded by each method and the computational time employed in their solution, two sets of tests are performed. In the first set, the OWC employed in Iturrioz et al. (2014) is used to analyse different cases. The heave of the OWC is studied as the heave movement of the mass of water inside the OWC at still water level (SWL). The first case is a decay test where results are compared with those obtained by IH-2VOF (Losada et al. 2008). In the second test, the RAO is produced with each radiation method, and the result compared with the RAO given by the BEM model used. Sensitivity of the results to t^* and the value of Δt used to precompute the *irf* are presented in this second test. The last case of study employing the OWC is an irregular sea state. This case requires the calibration of linear and nonlinear friction coefficients to compare the results with those obtained by IH-2VOF (Iturrioz et al. 2014). In all cases, the computational cost of solving the final system of ODEs obtained with each method is compared.

In the second set, the three methods were used in the study of a heave decay of the SPAR buoy based on the Hywind offshore wind project. The results are compared with data from laboratory experiments.

In order to study the sensitivity of each method to the set of frequencies provided, different sets of frequencies have been employed. Three different cases have been considered:

- An interpolation of the results given by the BEM model to 512 equally spaced frequencies between the minimum and the maximum frequencies used by the BEM model (for OWC, $\omega \in [1.532, 12.566]$, $\Delta\omega = 0.0216$). This set is called ‘Interpolated’.
- An interpolation of the results given by the BEM model to 512 equally spaced frequencies between the minimum frequency and 0.6 times the maximum frequency used by the BEM model (for OWC, $\omega \in [1.532, 7.540]$, $\Delta\omega = 0.0118$). This set is called ‘Truncated high’.
- An interpolation of the results given by the BEM model to 512 equally spaced frequencies between 1.5 times the minimum frequency and the maximum frequency used by the BEM model (for OWC, $\omega \in [2.299, 12.566]$, $\Delta\omega = 0.0201$). This set is called ‘Truncated low’.

This way, the influence of selected frequencies in the BEM execution can be evaluated.

3.1 Oscillating water column

In this section, the study carried out for an OWC device is described. All OWC cases were analysed with volume, $V = 20 \times 30 \times 68 \text{ cm}^3$, and added mass at infinity frequency $A_\infty = 31.43 \text{ kg}$ (Iturriz et al. 2014). The computational cost of solving the final system of ODEs obtained with each method and for every test is presented. The solution of all the systems of ODEs is done using the implicit Adams method with relative tolerance of 10^{-7} and absolute tolerance of 10^{-9} (Brown et al. 1989; Hindmarsh 1983).

In the case of the SS, the Matlab MSS FDI toolbox provided by Perez and Fossen (2009) was translated to Python and used. This toolbox is used in the identification of radiation-force models and fluid memory effects. The following characteristics were used in the MSS FDI toolbox:

- Method of resolution using the identification toolbox: 2
- Maximum order of the identification: 20
- Identification threshold: 0.99
- Number of iterations for the identification = 50.

The SS converges with third-order polynomials, while Prony only requires second-order ones to converge. This means that for IRF, the system of ODEs is of order 2, while in the SS the order is 5 and in Prony the order is only 4.

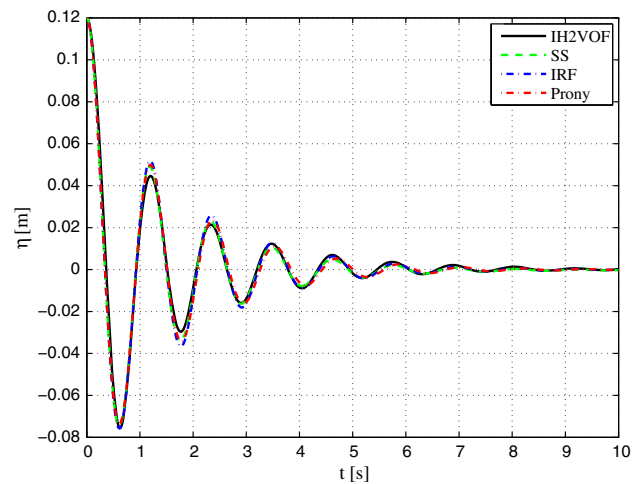


Fig. 5 Comparison of the results produced by IH-2VOF, state space, IRF and Prony's method using $\Delta t = 0.02 \text{ s}$ for a decay test with fluid memory $t^* = 3 \text{ s}$

3.1.1 Decay

The first comparison uses a decay test in heave, where the free surface is initially located outside of the equilibrium condition. The free surface is released and the system will evolve until the equilibrium condition is reached. The results produced by the three methods are compared with in-house CFD software IH-2VOF, (Losada et al. 2008). In order to adjust the results, calibration coefficients for the linear and non-linear frictions are included, $k_l = 25.0$ and $k_{nl} = 1$ (Iturriz et al. 2014). All methods produce results in good agreement with IH-2VOF, starting from an initial elevation of 0.12 m, as can be seen in Fig. 5. In Fig. 5, the time step considered is $\Delta t = 0.02 \text{ s}$ and fluid memory is $t^* = 3 \text{ s}$ when solving IRF and Prony. The effects of Δt and t^* for IRF are presented later.

All simulations, IRF, SS and Prony, have been repeated using the different sets of frequencies described above: ‘Interpolated’, ‘Truncation high’ and ‘Truncation low’. The results of those frequency schemes can be found in Fig. 6, where all cases yield very similar results. The natural period of each case is extracted from the corresponding decay test and the results are presented in Table 2. The only method showing slight variability in the results is the approximation by SS. Both IRF and Prony show no difference in the resulting natural period in any case. The results obtained from the three methods employed are very similar to one another. A summary of the executed cases for the heave decay of the OWC can be seen in Table 3.

In order to highlight the differences, the integral of the velocity of the free surface has been also computed for each case,

$$D(t) = \int_0^t \dot{\eta}(t) dt. \quad (24)$$

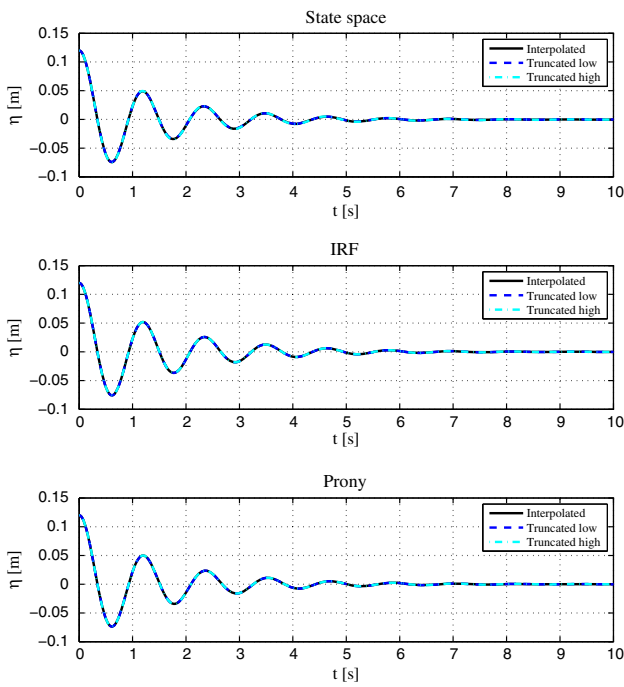


Fig. 6 Comparison of the results obtained by each method when pre-processing the BEM data using $\Delta t = 0.02$ s for a decay test with fluid memory $t^* = 3$ s

Table 2 Natural period, in seconds, obtained by each method and every pre-processing studied to compute the corresponding decay test

	SS	IRF	Prony
Interpolated	1.145	1.15	1.166
Truncated high	1.143	1.15	1.166
Truncated low	1.146	1.15	1.166

Table 3 Summary of the executed cases for the heave decay of the OWC

	Radiation method	Frequencies	t^* (s)	Δt (s)
OWC	SS	Interpolated	3	0.02
		Truncated high	3	0.02
		Truncated low	3	0.02
	IRF	Interpolated	3	0.02
			10	0.02
			3	0.01
Prony	Truncated high	3	0.02	
	Truncated low	3	0.02	
	Truncated low	3	0.02	

The comparison of the integrated values, $D(t)$, is shown in Table 4, where the only method yielding different results is the SS.

Table 4 Integral of the velocity of the free surface along the executed time normalised with the initial position of the OWC, 0.12 m

	SS	IRF	Prony
Interpolated	5.61×10^{-2}	7.07×10^{-2}	7.63×10^{-2}
Truncated high	2.99×10^{-2}	7.07×10^{-2}	7.63×10^{-2}
Truncated low	4.78×10^{-2}	7.07×10^{-2}	7.63×10^{-2}

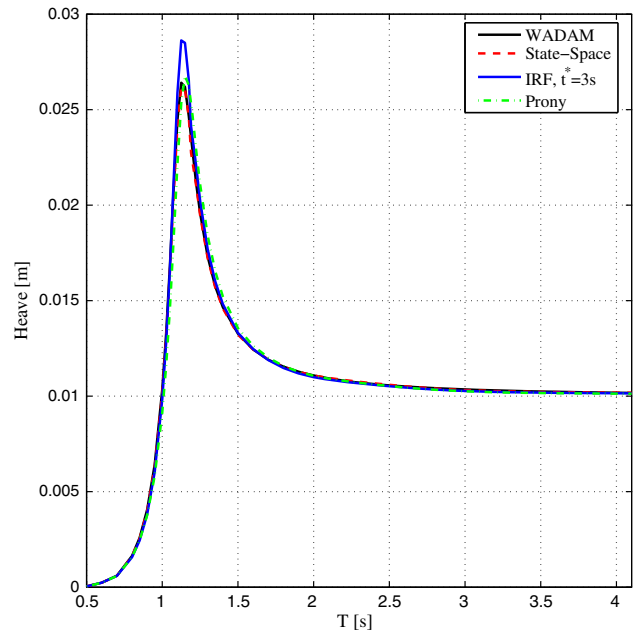


Fig. 7 Comparative results obtained by BEM, IRF, SS and Prony's method using $\Delta t = 0.02$ s

Table 5 Computational effort, in seconds, required by each method to compute the corresponding RAO

	SS	IRF ($t^* = 10$ s)	IRF ($t^* = 3$ s)	Prony
CPU (s)	32	55	37	32

3.1.2 RAO

A set of 47 frequencies, between 1.53 and 12.56 rad/s, were used in the BEM model. In order to reproduce the RAO, 47 simulations of regular waves were executed, using the frequencies studied in the BEM model.

Each regular wave train is simulated for 300 s using $\Delta t = 0.02$ s in all cases. To compute the RAO, only the last half of each simulation is used, since the steady state is reached. The obtained results are presented in Fig. 7. The corresponding computational costs are shown in seconds in Table 5. These computational costs include the whole simulation process: the computation of the *irf*, the state space identification, if required, or the Prony's approximation, if required, and the simulations of the 47 wave conditions.

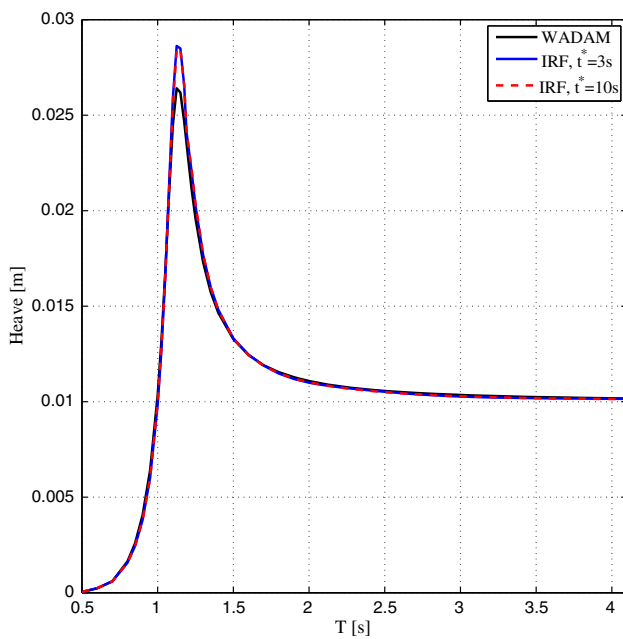


Fig. 8 Comparative results produced by BEM and IRF when using two different values for the memory of the fluid, $t^* = 3$ s and $t^* = 10$ s

Two values for the memory of the fluid are considered when computing the *irf*, $t^* = 3$ s and $t^* = 10$ s. These values are selected by inspection of Fig. 2. The RAOs obtained with this time history reduction are very similar one another as shown in Fig. 8. Using $t^* = 3$ s significantly reduces the computational cost of IRF to a similar cost as SS or Prony.

The largest error in Fig. 7 is caused by the direct calculation of the convolution integral. When computing this integral, the *irf* is precomputed for a set of time steps in $[0, t^*]$ with a fixed time step, Δt . This error is larger when more rapid changes in the velocity are produced, such as at the natural period of the OWC. This can be seen in Fig. 7. To reduce this error a smaller time step, Δt , is needed. The results obtained for time steps $\Delta t = 0.02$ s and $\Delta t = 0.01$ s are presented in Fig. 9, where the improvement is clearly observed. However, dividing the time step by two doubles the computational effort.

The RAOs have been repeated using the different sets of frequencies described before: ‘Interpolated’, ‘Truncation high’ and ‘Truncation low’. In case of IRF, two temporal discretizations are included $\Delta t = 0.02$ s and $\Delta t = 0.01$ s. The results can be seen in Fig. 10, where the differences in the amplitude at the natural period are in the order of 6% when using the different sets of frequencies for the SS method.

The IRF has also shown a 10% error with the RAO given by the BEM model, when using a large value of Δt . Neither IRF nor Prony seems to be sensitive to the change of frequencies. On the other hand, SS and Prony have not shown any sensitivity to the time step used, $\Delta t = 0.02$ s and $\Delta t = 0.01$ s.

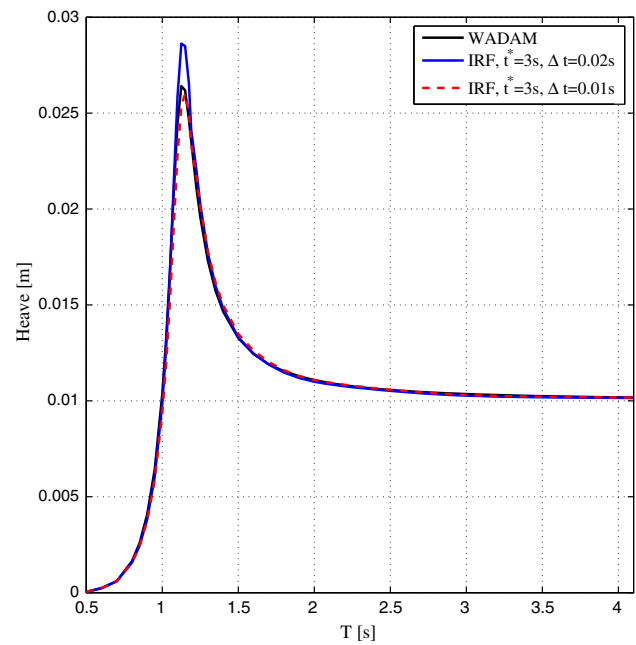


Fig. 9 Comparative results produced by BEM and IRF when using two different values for the time interval, $\Delta t = 0.02$ s and $\Delta t = 0.01$ s

A summary of the executed cases for the RAOs of the OWC is presented in Table 6.

3.1.3 OWC under irregular waves

The in-house CFD model IH-2VOF (Losada et al. 2008) is used to compare the results of the OWC under the action of an irregular sea state. In this case, a peak period of $T_p = 3.2$ s with significant wave height, $H_s = 0.06$ m, is run for 150 s using $\Delta t = 0.02$ s. The calibration of the linear and non-linear friction coefficients produced the values $k_l = 147.01$ and $k_{nl} = 0$ (Iturriz et al. 2014). The computational effort required for each method to compute the resulting system of ODEs is presented in Table 7. SS and Prony require similar computational cost, which is almost half the computational time required by the best case of IRF. The results obtained are compared in Fig. 11, where solutions from all methods are expressed. The results are similar to one another even using $\Delta t = 0.02$ s.

The movements of the OWC under irregular waves are computed using the superposition principle. Data from the BEM code are obtained for a set of frequencies. A different set of frequencies is obtained from the spectral decomposition of irregular waves, so interpolation is required from the known frequencies used in the BEM model. Small discrepancies can result specially in the interpolated phase as they are 2π periodic. The time series presented is $t \in (50, 100)$, so small differences in the interpolated phases could cause small discrepancies in the phase, as in Fig. 11. So, this time lag

Fig. 10 Comparative results obtained by BEM and IRF when using two different values for the time interval to obtain the solution $\Delta t = 0.02$ s and $\Delta t = 0.01$ s

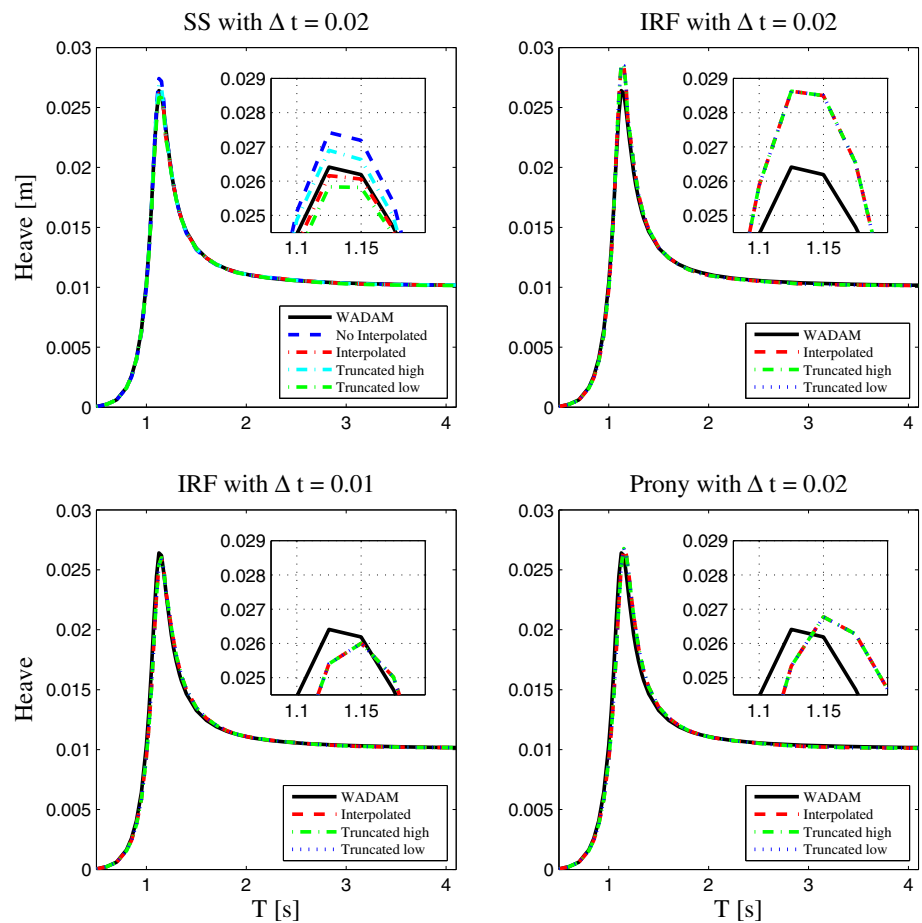


Table 6 Summary of the executed cases for the RAOs of the OWC

	Radiation method	Frequencies	t^* (s)	Δt (s)
OWC	SS	Interpolated	3	0.02
		Truncated high	3	0.02
		Truncated low	3	0.02
	IRF	Interpolated	3	0.02
			3	0.01
		Truncated high	3	0.02
			3	0.01
		Truncated low	3	0.02
			3	0.01
Prony	Interpolated	3	0.02	
	Truncated high	3	0.02	
	Truncated low	3	0.02	

Table 7 Computational effort required by each method to compute the resulting system of ODEs for each method in the case of irregular waves

	SS	IRF ($t^* = 10$ s)	IRF ($t^* = 3$ s)	Prony
CPU (s)	0.164	0.484	0.284	0.16

3.2 SPAR buoy

In this section, the analysis carried out for a SPAR buoy is described. A SPAR buoy based on the Hywind offshore wind project is used in this calibration because of the availability of laboratory results. In this study, three different BEM files have been applied: one using equidistant frequencies between 0.1 and 5 rad/s every 0.1 rad/s called ‘Original’; one using equidistant periods between 1 and 60 s every second called ‘Equal’; and finally, one with variable increments between 1 and 60 s, smaller close to the natural period and larger increments for the rest of periods called ‘Variable’. Infinity added mass has been externally computed to adjust the laboratory peak period in all the cases. Furthermore, linear and nonlinear coefficients are also used to adjust the damping measured at the laboratory, with the same coefficients in all simulations, $k_l = 2 \times 10^4$ and $k_{nl} = 4 \times 10^4$ (Iturrioz et al. 2014).

is the same in all three methods, because the lag comes from the wave excitation force, which is the same in all methods.

Previous tests have shown the sensitivity of IRF to the time step, but in this case the agreement is very good because the peak period of the waves is far from the natural period of the volume.

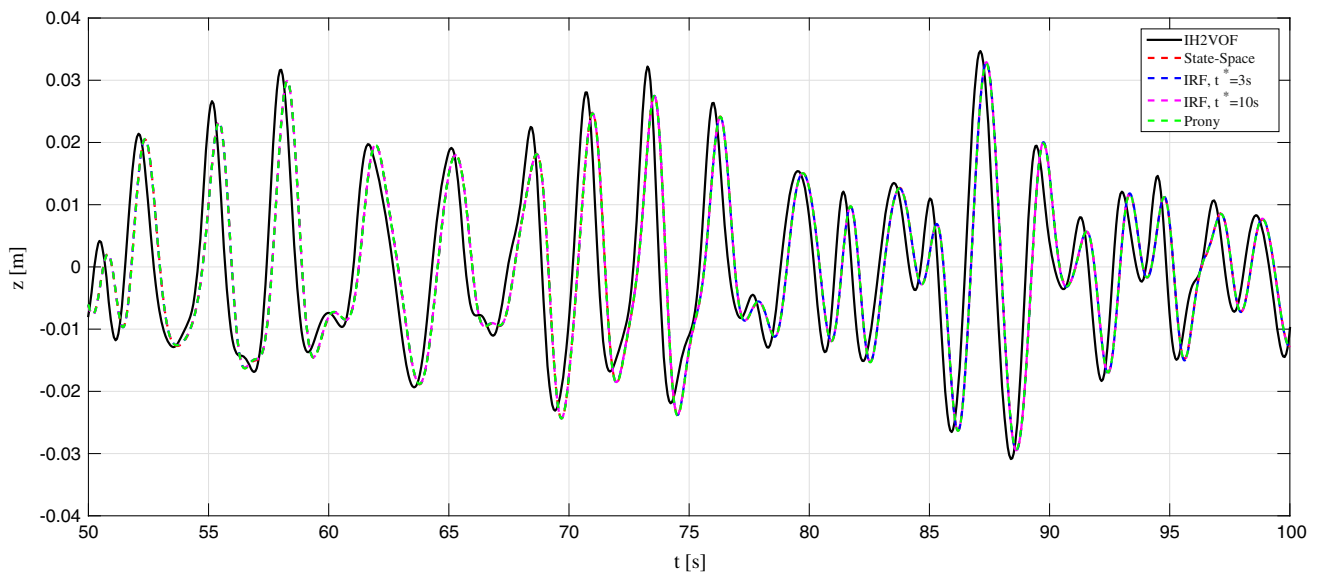


Fig. 11 Comparative of the results produced by IH-2VOF and those by IRF, state space and Prony’s method using $\Delta t = 0.02$ s

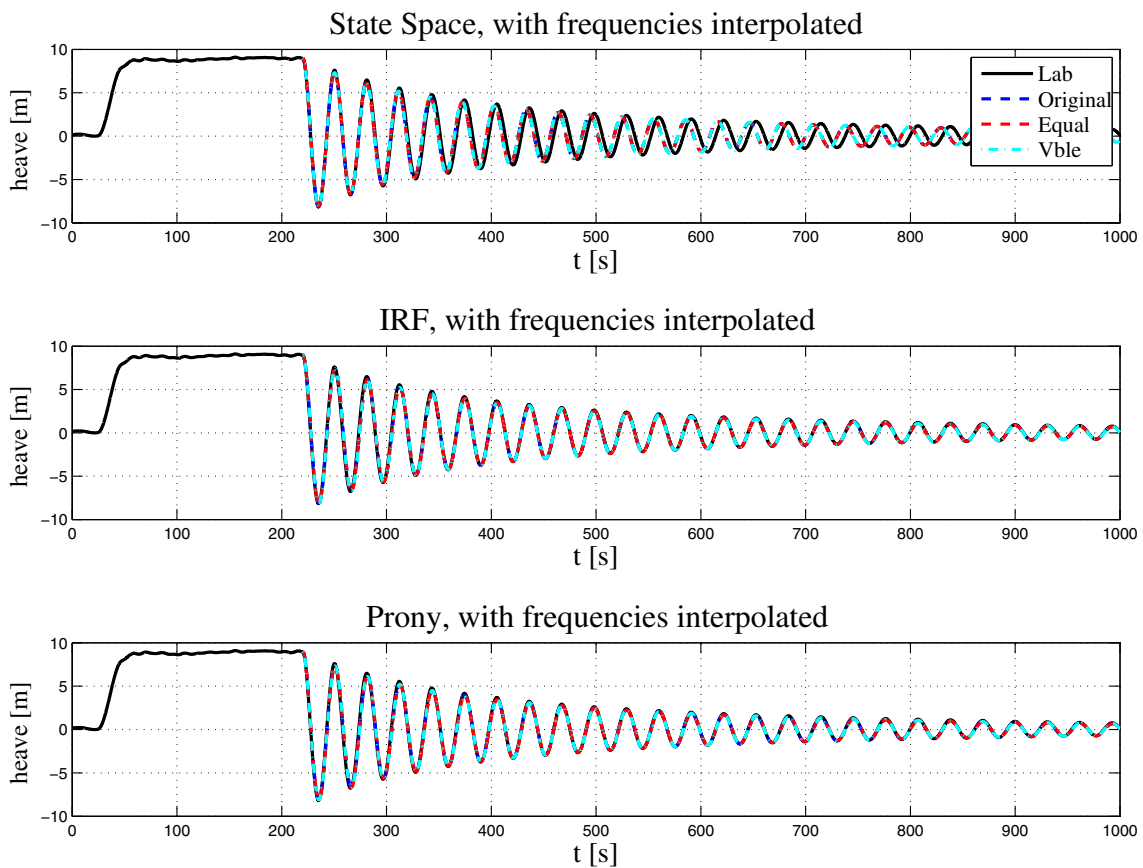


Fig. 12 Comparison of the results from a decay test in heave in the laboratory and those produced by different methods to compute the radiation (*top* state space, *middle* IRF, *bottom* Prony) for the three BEM files

For every radiation method, all BEM cases have been studied. Figure 12 presents the results of a decay test of the SPAR buoy in heave (initial condition $z = 9$ m). Laboratory results

are compared with those obtained from interpolated BEM data, 512 equidistant frequencies, when using the different methods to calculate the convolution integral presented in this

Table 8 Natural period, in seconds, obtained by each method and every BEM file to compute the corresponding decay test of the SPAR buoy

	SS	IRF	Prony
Original	30.464	30.91	30.918
Equal	30.464	30.91	30.918
Variable	30.447 ^a	30.91	30.932 ^a

^a The cases where convergence is not reached in the identification of the SS or Prony

Table 9 Computational effort, in seconds, required by each method to compute the system of ODEs for the corresponding data from BEM

	SS	IRF ($t^* = 30$ s)	Prony
Original	0.76 (8)	0.17 (2)	0.46 (22) ^a
Equal	1.97 (8)	0.18 (2)	0.37 (18)
Variable	3.22 (22) ^a	0.16 (2)	0.39 (18)

The order of the resulting ODEs system is presented in between parentheses.

^a The cases where convergence is not reached in the identification of the SS or Prony

article. Table 11 shows that SS yields small errors when capturing the natural period, while IRF and Prony approximate it well. Table 8 presents the natural periods obtained from each method for every BEM file. Results in the table show small sensitivity on the BEM files in the case of SS and Prony, in which convergence is not reached in the identification of the coefficients marked with the letter a symbol. The different BEM files and the interpolation seem to have no effect on the final result obtained with each method. Computational costs employed for each method are shown in Table 9, in which the letter a represents the cases where convergence is not reached in the identification of the coefficients.

The data used to interpolate the coefficients of SS and Prony in the study of the OWC are also used for the SPAR buoy. This means that the maximum order employed in these simulations is 20. The total order of the ODEs system obtained by each method is shown in parentheses in the table. It is obvious that the order of IRF is always 2, but there is a variability in the order used in SS and Prony. This variability is reflected in the computational effort required by each method. The changes in the data used from the BEM model have no influence on the matrix of the system in the IRF method. This is explained because the radiation force is calculated in the RHS of the system, and small discrepancies are not reflected in the solution of the system. On the other hand, SS and Prony compute the radiation term modifying the matrix of the ODEs system. Small changes in the matrix coefficients can modify the properties of the matrix. Such changes will be reflected in the computation of the ODEs system. In the presented analysis of the SPAR buoy, the com-

putational cost of IRF remains almost constant, always lower than the computational cost of SS and Prony.

For the case of ‘Equal’, the test cases have been repeated using the 6 DOFs of the platform instead of only heave. The order of the matrix for IRF is obviously 12 and the computational cost required is 2.6 s. For SS, the order is 112 with a computational effort of 1011 s. Prony requires an order of the matrix of 76 and a computational effort of 4.8 s. The final ODEs system generated by every method is computed by the implicit Adams method that uses variable time steps. The use of variable time steps requires less computational steps when the matrix of the system has appropriate eigenvalues. These eigenvalues change as the coefficients of the matrix vary, due to the different results of the approximations in SS and Prony. IRF and Prony’s methods require similar numbers of evaluations, while SS requires between 2 and 8 times more evaluations of the system matrix for the simulated cases. Every execution simulates 1800 s, writing results every 0.1 s.

Once the comparison of different BEM files was completed, a new set of simulations were executed only with BEM file ‘Equal’ (periods between 1 and 60 s every second). The simulations comprise different interpolations of the set of frequencies given by the BEM model. The first interpolation is between the initial and final frequencies given by BEM (0.1 and 6.28 rad/s). In the second interpolation the upper frequencies are truncated to 1.5 rad/s ($T = 4.19$ s) and in the third interpolation the lower frequencies are truncated only to 0.175 rad/s ($T = 35.9$ s), as the natural frequency is slightly larger than 0.2 rad/s. A summary of the executed cases for the SPAR can be seen in Table 10. Figure 13 shows that interpolation and low-frequency truncation seem to have

Table 10 Summary of the executed cases for the SPAR

	Radiation method	BEM	Frequencies
SPAR	SS	Original	
		Equal	Interpolated
			Truncated high
			Truncated low
		Variable	
	IRF	Original	
		Equal	Interpolated
			Truncated high
			Truncated low
		Variable	
Prony	Original		
	Equal	Interpolated	
		Truncated high	
		Truncated low	
	Variable		

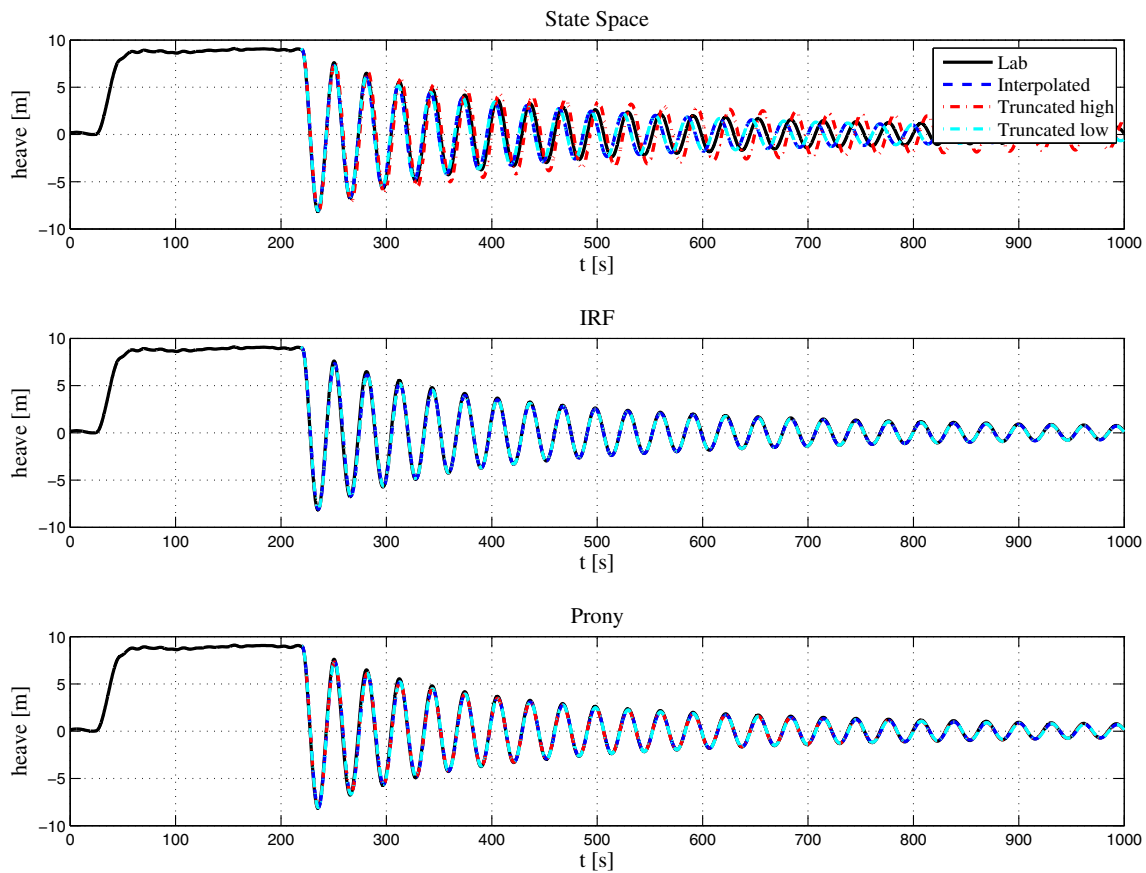


Fig. 13 Comparative results from a decay test in heave in the laboratory and those yielded by different methods to compute the radiation (*top* SS, *middle* IRF, *bottom* Prony) for the BEM files with equidistant periods. Different frequencies interpolations are presented

Table 11 Natural period, in seconds, obtained by each method and every pre-processing studied to compute the corresponding decay test of the SPAR buoy

	SS	IRF	Prony
Interpolated	30.464	30.91	30.932
Truncated high	31.226	30.91	30.914
Truncated low	30.464	30.91	30.932

no effect on the results for any method. On the other hand, the high-frequency truncation seems to have a strong effect on the results of SS. This effect starts with the identification process, as it fails to converge when the 4 larger frequencies are removed from the interpolation. Natural periods obtained for every decay test are presented in Table 11. As can be observed, this time the IRF is the only method that yields the same results in all cases. The differences obtained by SS or Prony are tiny, except in the case of ‘Truncated high’ for the SS. This was not unexpected as, convergence was not reached in the approximation of the polynomials in that case. The proposed truncations, of low and high frequencies, seem to have no influence on the solutions obtained by the IRF method. On the other hand, the results provided by SS and Prony

Table 12 Computational effort, in seconds, required by each method to compute the corresponding interpolated and truncated data BEM model “equal”

	SS	IRF ($t^* = 30$ s)	Prony
Interpolated	1.97 (8)	0.18 (2)	0.37 (18)
Truncated high	0.37 (22) ^a	0.16 (2)	0.36 (18)
Truncated low	2.06 (8)	0.17 (2)	0.37 (18)

The time needed to calculate the final system is presented with the order of the system between parentheses.

^a The cases where convergence is not reached in the identification of the state space

have shown some small impact on the pre-processing performed. The computational cost of these sets of comparisons can be seen in Table 12 and they follow the same pattern as in Table 9, IRF being the fastest one.

4 Conclusions

The three methods employed in the literature to evaluate the convolution term of Cummins’ equation have been implemented and compared. The computation of the *irf* has been

extended to infinity, interpolating the data obtained by a BEM and analytically solving the integral to infinity avoiding truncation errors (Kashiwagi 2004). The systems of ODEs resulting in each method are computed using the same numerical algorithm. The solutions obtained by all methods are similar to one another.

In order to save computational time, the *irf* values are precomputed for a predefined interval with a fixed time step (Kurniawan et al. 2011). The results obtained by IRF have shown sensitivity to the value of the chosen time step. Large time steps yielded errors around the natural period of the structure under study. On the other hand, their results have not shown sensitivity to different BEM files or to the pre-processing performed to BEM data.

SS method has shown two issues. The first one is the sensitivity of the results to the pre-processing of BEM data in both the decay test and RAOs of the OWC. The differences in the results have always been very small. The second issue is that using the same parameters for identification, the method converged for BEMs cases ‘Original’ and ‘Equal’, but failed to converge in the case ‘Variable’. The only thing that changed for different BEM cases is the set of predefined frequencies chosen.

The Prony method has also shown sensitivity in the results when pre-processing BEM data in the case of the spar buoy, but differences in the results are very small.

The change on the data used from the BEM model has no influence on the matrix of the system in the IRF method. Radiation force is evaluated at the right-hand side of the system, and small discrepancies are not reflected on the solution of the system, as the matrix characteristics remain the same. SS and Prony calculated the radiation term modifying the matrix and, therefore, the characteristics of the ODEs system. In conclusion, small changes will be reflected in the solution of the system. Hence, both systems show errors appearing in the solution of the radiation term.

The simulations performed by SS and Prony’s approximations have been computationally cheaper than those by IRF in the cases of the OWC. On the other hand, IRF was computationally cheaper than Prony and SS approximations in the case of the SPAR decay. This seems to highlight that SS and Prony are quicker when the identification is carried out with polynomials of low order and IRF is quicker if high order is needed for the identification. When using more DOFs in the study, the order of the system increases much more in SS and Prony than in IRF, which makes IRF quicker.

With the increase of computational capabilities given by actual computers, the authors recommend the use of direct integration method to compute the radiation term in Cummins’ equation, avoiding the uncertainties seen in the identification of the coefficients in the SS and Prony’s methods. However, a mention has to be made to highlight that the solution given by SS or Prony’s methods should be consid-

ered in those cases where the access to modern computational capabilities is reduced.

Acknowledgments The authors are grateful to the Spanish Ministry of Economy and Competitiveness and in particular to the State Secretariat for the Research, Development and Innovation funding for VAPEO-Ocean Climate Variability influence over Wave Energy Converters Power Production project (ENE2013-48716-R), within the National Programme for Research Aimed at the Challenges of Society, modality 1, Research Challenge: Research, Development and Innovation.

Appendix: Primitive of the infinite integral

The equation to be solved is

$$\int ae^{b\omega} \cos(\omega t) d\omega. \tag{25}$$

Applying integration by parts with

$$u = \cos(\omega t); \quad dv = ae^{b\omega} \Rightarrow du = -t \sin(\omega t); \quad v = \frac{a}{b} e^{b\omega}, \tag{26}$$

the following is obtained:

$$\int ae^{b\omega} \cos(\omega t) d\omega = \cos(\omega t) \frac{a}{b} e^{b\omega} + \frac{t}{b} \int ae^{b\omega} \sin(\omega t). \tag{27}$$

Again, integration by parts over the resulting integral with

$$u = \sin(\omega t); \quad dv = ae^{b\omega} \Rightarrow du = t \cos(\omega t); \quad v = \frac{a}{b} e^{b\omega}, \tag{28}$$

results in

$$\int ae^{b\omega} \sin(\omega t) = \sin(\omega t) \frac{a}{b} e^{b\omega} - \frac{t}{b} \int ae^{b\omega} \cos(\omega t) \tag{29}$$

Writing all together and applying algebra,

$$\begin{aligned} \int ae^{b\omega} \sin(\omega t) &= \frac{a}{b} e^{b\omega} \cos(\omega t) + \frac{at}{b^2} \sin(\omega t) \\ &\quad - \frac{t^2}{b^2} \int ae^{b\omega} \sin(\omega t) \\ &\Rightarrow \left(1 + \frac{t^2}{b^2}\right) \int ae^{b\omega} \sin(\omega t) \\ &= \frac{a}{b} e^{b\omega} \cos(\omega t) + \frac{at}{b^2} \sin(\omega t) \\ &\Rightarrow \int ae^{b\omega} \sin(\omega t) \\ &= \frac{\frac{a}{b} e^{b\omega} \cos(\omega t) + \frac{at}{b^2} \sin(\omega t)}{\left(1 + \frac{t^2}{b^2}\right)}. \end{aligned} \tag{30}$$

References

- Abraham E, Kerrigan E (2013) Optimal active control and optimization of a wave energy converter. *Sustainable Energy, IEEE Transactions on* 4(2):324–332. doi:10.1109/TSTE.2012.2224392
- Alves MAA (2012) Numerical simulation of the dynamics of point absorber wave energy converters using frequency and time domain approaches. PhD thesis, Universidade Técnica de Lisboa
- de Andres AD, Guanche R, Armesto JA, del Jesus F, Vidal C, Losada IJ (2013) Time domain model for a two body heave converter: model and applications. *Ocean Engineering* 72:116–123
- Armesto JA, Guanche R, Iturrioz A, Vidal C, Losada IJ (2014) Identification of state-space coefficients for oscillating water columns using temporal series. *Ocean Engineering* 79(0):43–49. doi:10.1016/j.oceaneng.2014.01.013, <http://www.sciencedirect.com/science/article/pii/S0029801814000225>
- Babarit A, Clément AH (2006) Optimal latching control of a wave energy device in regular and irregular waves. *Applied Ocean Research* 28(2):77–91
- Babarit A, Clément AH, Ruer J, Tartivel C (2006) SEAREV: A fully integrated wave energy converter. In: *Proceedings of OWEMES*
- Babarit A, Hals J, Muliawan MJ, Kurniawan A, Moan T, Krokstad J (2012) Numerical benchmarking study of a selection of wave energy converters. *Renewable Energy* 41:44–63
- Bailey H, Bryden IG (2012) Influence of a quadratic power take-off on the behaviour of a self-contained inertial referenced wave energy converter. *Proceedings of the Institution of Mechanical Engineers, Part M: Journal of Engineering for the Maritime Environment* 226:15–22
- Brown PN, Byrne GD, Hindmarsh AC (1989) VODE: a variable-coefficient ODE solver. *SIAM Journal on Scientific and Statistical Computing* 10(5):1038–1051
- Chitrapu AS, Ertekin RC (1995) Time-domain simulation of large-amplitude response of floating platforms. *Ocean Engineering* 22(4):367–385
- Crozier R, Bailey H, Mueller M, Spooner E, McKeever P (2013) Analysis, design and testing of a novel direct-drive wave energy converter system. *Renewable Power Generation, IET* 7(5):565–573
- Cummins WE (1962) The impulse response function and ship motions. *Schiffstechnik* 9:101–109
- Duarte T, Alves M, Jonkman J, Sarmiento A (2013) State-space realization of the wave-radiation force within FAST. In: *Proceedings of the 32 International Conference on Ocean, Offshore and Arctic Engineering*
- Duclos G, Clément AH, Chatry G (2001) Absorption of outgoing waves in a numerical wave tank using a self-adaptive boundary condition. *International Journal of Offshore and Polar Engineering* 11(3):168–175
- Folley M, Babarit A, Child B, Forehand D, O'Boyle L, Silverthorne K, Spinneken J, Stratigaki V, Troch P (2012) A review of numerical modelling of wave energy converter arrays. In: *31st International Conference on Ocean, Offshore and Arctic Engineering*, pp 535–545
- Fusco F, Ringwood J (2011) Suboptimal causal reactive control of wave energy converters using a second order system model. In: *21st International Offshore and Polar Engineering Conference*, pp 687–694
- García N, Lara JL, Losada IJ (2004) 2-d numerical analysis of near-field flow at low-crested permeable breakwaters. *Coastal Engineering* 51(10):991–1020. doi:10.1016/j.coastaleng.2004.07.017
- Greenhow M (1986) High- and low-frequency asymptotic consequences of the kramers-kronig relations. *Journal of Engineering Mathematics* 20(4):293–306. doi:10.1007/BF00044607
- Grilli AR, Merrill J, Grilli ST, Spaulding ML (2007) Experimental and numerical study of spar buoy-magnet/spring oscillators used as wave energy absorbers. In: *Proc. 17th International Offshore and Polar Engineering Conference*, pp 486–489
- Guanche R, Losada IJ, Lara JL (2009) Numerical analysis of wave loads for coastal structure stability. *Coastal Eng.* doi:10.1016/j.oceaneng.2008.05.006
- Guanche R, Gómez V, Vidal C, Eguinoa I (2013) Numerical analysis and performance optimization of a submerged wave energy point absorber. *Coast Eng* 59:214–230
- Guanche R, Iturrioz A, Losada IJ (2015) Hybrid modeling of pore pressure damping in rubble mound breakwaters. *Coast Eng* 99:82–95
- Hindmarsh AC (1983) ODEPACK, a systematized collection of ODE solvers. In: Stepleman RS, Carver M, Peskin R, Ames WF, Vichnevetsky R (eds) *Scientific computing. IMACS transactions on scientific computation*, vol 1. North-Holland, Amsterdam, pp 55–64
- Hsu TJ, Sakakiyama T, Liu PLF (2002) A numerical model for wave motions and turbulence flows in front of a composite breakwater. *Coastal Engineering* 46(1):25–50. doi:10.1016/S0378-3839(02)00045-5
- Iturrioz A, Guanche R, Armesto JA, Alves MA, Vidal C, Losada IJ (2014) Time-domain modeling of a fixed detached oscillating water column towards a floating multi-chamber device. *Ocean Engineering* 76:65–74
- Jefferys E (1984) Simulation of wave power devices. *Applied Ocean Research* 6(1):31–39
- Jonkman J (2007) *Dynamics Modelling and Loads Analysis of an Offshore Floating Wind Turbine*. Tech. rep, National Renewable Energy Laboratory, USA
- Karimirad M (2013) Modeling aspects of a floating wind turbine for coupled wave-wind-induced dynamic analyses. *Renewable Energy* 53:299–305
- Kashiwagi M (2000) A time-domain mode-expansion method for calculating transient elastic responses of a pontoon-type vlfs. *Journal of Marine Science and Technology* 5:89–100
- Kashiwagi M (2004) Transient responses of a VLFS during landing and take-off of an airplane. *Journal of Marine Science and Technology* 9(1):14–23. doi:10.1007/s00773-003-0168-0
- de Kat JO (1988) Large amplitude ship motions and capsizing in severe sea conditions. PhD thesis, University of California
- Kristiansen E, Egeland O (2003) Frequency-dependent added mass in models for controller design for wave motion damping. In: Blanke M, Pourzanjani MMA, Vukić ZZ (eds) *Manoeuvring and Control of Marine Craft 2003 (MCMC 2003): A Proceedings Volume from the 6th IFAC Conference*. Elsevier
- Kristiansen E, Hjulstad A, Egeland O (2005) State-space representation of radiation forces in time-domain vessel models. *Ocean Engineering* 32(17–18):2195–2216
- Kurniawan A, Hals J, Moan T (2011) Assessments of time-domain models of wave energy conversion system. In: *Proceedings of the Ninth European Wave and Tidal Energy Conference*, University of Southampton, Southampton
- Kurniawan A, Pedersen E, Moan T (2012) Bond graph modelling of a wave energy conversion system with hydraulic power take-off. *Renewable Energy* 38(1):234–244
- Lara JL, Garcia N, Losada IJ (2006) Rans modelling applied to random wave interaction with submerged permeable structures. *Coastal Engineering* 53(5–6):395–417. doi:10.1016/j.coastaleng.2005.11.003
- Lara JL, Losada IJ, Guanche R (2008) Wave interaction with low-mound breakwaters using a rans model. *Ocean Engineering* 35(13):1388–1400. doi:10.1016/j.oceaneng.2008.05.006, <http://www.sciencedirect.com/science/article/pii/S0029801808001194>
- Liu PLF, Lin PZ, Chang KA, Sakakiyama T (1999) Numerical modelling of wave interaction with porous structures. *Journal of Waterways, Port, Coastal, and Ocean Engineering* 125(6):322–330

- Losada IJ, Lara JL, Christensen ED, Garcia N (2005) Modelling of velocity and turbulence fields around and within low-crested rubble-mound breakwaters. *Coastal Engineering* 52(10–11):887–913. doi:10.1016/j.coastaleng.2005.09.008
- Losada IJ, Lara JL, Guancho R, Gonzalez-Ondina JM (2008) Numerical analysis of wave overtopping of rubble mound breakwaters. *Coastal Engineering* 55(10):47–62
- McCabe AP, Bradshaw A, Widden M (2005) A time-domain model of a floating body using transforms. In: *Proceedings of the Sixth European Wave and Tidal Energy Conference*, University of Strathclyde, Glasgow
- Muliawan MJ, Karimirad M, Moan T (2013) Dynamic response and power performance of a combined Spar-type floating wind turbine and coaxial floating wave energy converter. *Renewable Energy* 50:47–57
- Nolte JD, Ertekin RC (2014) Wave power calculations for a wave energy conversion device connected to a drogue. *Journal of Renewable and Sustainable Energy* 6(1):013117
- Paul J (1998) *Modelling of General Electromagnetic Material Properties in TLM*. PhD thesis, University of Nottingham
- Perez T, Fossen TI (2008) Time-domain vs. frequency-domain identification of parametric radiation force models for marine structures at zero speed. *Modelling, Identification and Control* 29:1–19
- Perez T, Fossen TI (2009) A Matlab toolbox for parametric identification of radiation-force models of ships and offshore structures. *Modelling, Identification and Control* 30:1–15
- Perez T, Fossen TI (2011) Practical aspects of frequency-domain identification of dynamic models of marine structures from hydrodynamic data. *Ocean Engineering* 38:426–435
- Philippe M, Babarit A, Ferrant P (2013) Modes of response of an offshore wind turbine with directional wind and waves. *Renewable Energy* 49:151–155
- de Prony BGR (1795) Essai expérimental et analytique: sur les lois de la dilatabilité de fluides élastique et sur celles de la force expansive de la vapeur de l'alkool, à différentes températures. *Journal de l'école Polytechnique* 1(22):24–76
- Ricci P, Saulnier JB, de O Falcao AF, Pontes MT (2008) Time-domain models and wave energy converters performance assessment. In: *27th international conference on ocean, offshore and Arctic engineering*
- Schoen MP, Hals J, Moan T (2011) Wave prediction and robust control of heaving wave energy devices for irregular waves. *Energy Conversion, IEEE Transactions on* 26(2):627–638. doi:10.1109/TEC.2010.2101075
- Shires A, Collu M, Borg M (2013) FloVAWT: Progress on the development of a coupled model of dynamics for floating offshore vertical axis wind turbines. *23rd International Offshore and Polar Engineering Conference, International Society of Offshore and Polar Engineers (ISOPE)*. Anchorage, Alaska, USA, pp 345–351
- SIMO (2008) SIMO - Theory Manual version 3.6, rev: 1. Marintek
- Spyrou KJ, Tigkas IG (2011) Nonlinear surge dynamics of a ship in astern seas: Continuation analysis of periodic states with hydrodynamic memory. *Journal of Ship Research* 55(1):19–28
- Taghipour R, Perez T, Moan T (2008) Hybrid frequency-time domain models for dynamic response analysis of marine structures. *Ocean Engineering* 35:685–705
- WADAM (2014) SESAM Users manual, WADAM. WWW page, <http://www.dnv.com>, accessed Dec 2014
- WAMIT (2014) WAMIT Users manual. WWW page, <http://www.wamit.com>, accessed Dec 2014
- Yu X, Falzarano JM, Su Z (2010) Time-domain simulation of a multi-body floating system in waves. *Proceedings of the 29 International Conference on Ocean, Offshore and Arctic Engineering, ASME, Shanghai, China*, pp 797–803
- Yu Z, Falnes J (1995) State-space modelling of a vertical cylinder in heave. *Applied Ocean Research* 17(5):265–275
- Yu Z, Falnes J (1998) State-space modelling of dynamic systems in ocean engineering. *Journal of Hydrodynamics, Serie B* 1:1–17